Isı Bilimi ve Tekniği Dergisi, 29, 2, 01-09, 2009
J. of Thermal Science and Technology

ISSN 1300-3615

SEAWATER DESALINATION IN A DIRECT CONTACT HEAT EXCHANGER: GLOBAL AND LOCAL MODEL RESULTS

Murat TEKELİOĞLU
Mechanical Engineering Department, University of Nevada, Reno, NV 89557 USA,
tekelioglu_murat@yahoo.com

(Geliş Tarihi: 23. 12. 2008, Kabul Tarihi: 19. 03. 2009)

Abstract: As the world population and the industrial and residential demands increase, it becomes important to compensate for the potable water shortage. To overcome the aforementioned crisis, several desalination techniques have been used for many years. In this work, we develop and implement global and local models to manifest the effectiveness of direct contact heat exchange in desalination of seawater. Direct contact processes offer many advantages such as low cost, absences of scale build-up and resistance of the heat transmitting material. The global model results show that about 65% of thermal seawater evaporation is possible. Local model, based on evaporation of one single droplet, was used to establish sizing parameters on the heat exchanger, e.g., evaporator length, cross-section area, and volume. It was shown of the seawater to have a short evaporation length.
Keywords: Direct contact heat transfer, Seawater, Desalination, Evaporation.

DENİZ SUYUNUN BİR DİREK TEMAS ISI DEĞİŞTİRİCİSİNDE ARITILMASI: GLOBAL VE LOKAL MODEL SONUÇLARI

Özet: Dünyadaki nüfus ve endüstriyel ve konutlardaki talep artışları arttıkça, içme suyu ihtiyacının karşılanması önemli olmaktadır. Bu problemin etkilerini azaltmak amacı ile, çeşitli tuzlu su arıtma projeleri yıllardan beri uygulanmaktadır. Bu çalışmada, direk temas ısı değiştirme etkinliğini deniz suyu arıtılmasında göstermek amacıyla, global ve lokal modeller geliştirip uygulamaktayız. Direk temas ısı transfer prosesleri bir çok avantajlar sunar: düşük maliyet, ısı transfer yüzeyinde tortu birikiminin olmaması ve ısı transferi direncinin bulunmaması gibi. Genel model sonuçları, proseste, yaklaşık %65 deniz suyu thermal buharlaşmasının mümkün olduğunu göstermektedir. Bir tek damlacığın buharlaşmasını temel alan lokal model, ısı değiştiricisi boyutlarının (uzunluk, kesit alanı, ve hacim) belirlenmesinde kullanılmıştır. Deniz suyunun, kısa bir buharlaşma mesafesi olduğu gösterilmiştir.
Anahtar kelimeler: Direk temas ısı transferi, Deniz suyu, Tuzlu su arıtılması, Buharlaşma.

NOMENCLATURE

Letter

A	Cross-section area [m^2]
a	Effective heat transfer surface area [m^2]
g	Gravitational acceleration [N/kg]
h	Enthalpy [kJ/kg]
h	Convective heat transfer coefficient [$W/(m^2K)$]
L	Vapor layer thickness [mm]
$LMTD$	Logarithmic mean temperature difference [ΔK or $\Delta^\circ C$]
$\dot{M}$	Mass flux [$kg/(s \cdot m^2)$]
$\dot{m}$	Mass flow rate [kg/s]
p	Pressure [N/m^2]
r	Ellipsoidal half-width [mm]
T	Temperature [K]
t	Time [s]
U	Velocity [m/s]
U	Heat transfer coefficient [$W/(m^2 \cdot K)$]
u	X- component of the velocity [m/s]
$\bar{u}$	Mean (average) velocity [m/s]
V	Volume [$liter$]
v	Y- component of the velocity [m/s]
v	Superficial velocity, $\dot{m}/(\rho \cdot A)$ [m/s]
w	Z- component of the velocity [m/s]
x	Length [m]

Greek

ε	Void fraction [%]
μ	Dynamic viscosity [$Pa \cdot s$]
ϕ	Salinity [% mass]
ρ	Density [kg/m^3]

Subscript

atm	Atmospheric
b	Brine
b	Beneath
c	Continuous phase
cp	Combustion products
C_3H_8	Propane
CO_2	Carbon dioxide
d	Dispersed phase
e	Evaporator
f	Liquid
fg	Liquid-to-gas
$H_2O(g)$	Water vapor (combustion products)
m	Mean (average)
N_2	Nitrogen
o	Outer
o	Initial
p	Products
p	Constant pressure
R	Reference
s	Surface
s	Saturated
sw	Seawater
t, *wv*	Total water vapor
v	Vapor
v	Volumetric
wv	Water vapor

INTRODUCTION

In contrast to the rising problem of potable water shortage, most of the world surface is covered by water. However, the world's 94% of available water is salty and only 6% is fresh (International Desalination Association (IDA), 2000). Further, 72% of the latter is underground and 27% is in glaciers. Therefore, to solve the problem of potable quality water shortage, it is suitable to implement desalination methods to turn the saline water into a potable water source. This process also benefits the agriculture.

Installed capacity of the desalination plants, from most-to-the-least, were given as multi-stage flashing (44%), reverse osmosis (42%), electro dialysis (6%), multi-effect distillation (4%), and vapor-compression (4%) (IDA, 2000). It was noted that the total production capacity of the multi-stage flashing (MSF) and reverse osmosis (RO) systems were competitive with $9.8 \cdot 10^6 m^3 / day$ versus $9.6 \cdot 10^6 m^3 / day$ as of 1997.

A research overview on the processes of MSF and RO systems was presented (Khawaji et al., 2008). Thermal and membrane systems and other alternative methods were discussed under the economics of such plants. The fouling of membrane in membrane distillation (MD) systems was studied (Hsu et al., 2002). The aim was to distill the raw seawater, a NaCl solution, and a pre-treat water in MD and compare the permeate fluxes ($kg/(m^2 h)$) with presence of fouling at the membrane surface. They observed with the raw seawater, nearly half permeate flux (more fouling) compared to NaCl solution. They applied ultrasound cleaning technique to the membrane to overcome the fouling. A similar MD process was investigated (Termpiyakul et al., 2005). A membrane distillation coefficient (C, $kg/(m^2 \cdot h \cdot Pa)$) was found on pure water and the other C values were estimated for high salt concentrations (up to 35,000 mg/L). In the other study, theoretical and experimental values of condensation and evaporation coefficients were included (Marek and Straub, 2001). They pointed out the real gas effects in the processes and found that the condensation coefficient for water was greater than its evaporation coefficient. A theoretical model for the evaporation of dispersed volatile drops in direct contact of a continuous immiscible liquid was described (Kendoush, 2004). The author developed heat transfer coefficients for n-pentane and n-butane coolant drops. Direct contact MD was given (Yun et al., 2006) for high-concentration NaCl solutions from theoretical and experimental aspects.

In this paper, we investigate the effectiveness of direct contact heat exchange process in seawater desalination. A spray- column was used. With two types of fuels (Hydrogen and Propane) tested on two models (global and local), the outcomes aimed to determine the amount of water vapor out of seawater evaporation and evaporator dimensions such as length, cross-section area, and volume

GLOBAL MODEL

A schematic direct-contact heat-exchanger (DCHX) is shown in Fig. 1. The combustion products enter in the spray-column and rise toward the falling-off seawater droplets from a sprinkler system and give their heat to the seawater. The evaporated seawater (water vapor) is received from the top and the much denser brine (in salt content) is delivered from the bottom of the system. The sensible cooling of the combustion products is the onset for the seawater mass transfer (latent heat). The water vapor received from the top of the heat exchanger is condensed in a condenser. A pre-heater can also replace the condenser, which preheats, e.g., the incoming seawater up to its temperature of saturation.

Applying the first law of thermodynamics to the system shown in Fig. 1, we get

$$\dot{m}_{sw} h_{sw} + \dot{m}_{cp} h_{cp} = \dot{m}_p h_p + \dot{m}_b h_b \qquad (1)$$

where $\dot{m}_{sw}$ is the seawater mass flow rate (kg/s), h_{sw} is the seawater enthalpy (kJ/kg), $\dot{m}_{cp}$ is the mass flow rate of the combustion products (kg/s), h_{cp} is the enthalpy of the combustion products

(kJ/kg), $\dot{m}_p$ is the mass flow rate of the products (kg/s), h_p is the enthalpy of the products (kJ/kg), $\dot{m}_b$ is the brine mass flow rate (kg/s), and h_b is the brine enthalpy (kJ/kg). The two mass balance equations give

$$\dot{m}_{sw} + \dot{m}_{cp} = \dot{m}_b + \dot{m}_p \tag{2}$$

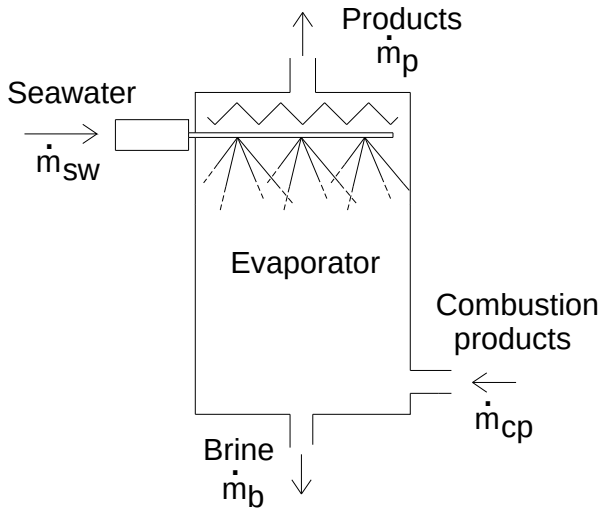

Figure 1. Schematic of the direct contact heat exchanger with input and output.

where $\dot{m}_p$, $\dot{m}_p = \dot{m}_{cp} + \dot{m}_{wv}$ is comprised of the both combustion products and water vapor of seawater evaporation

$$\dot{m}_{sw} = \dot{m}_b + \dot{m}_{wv} \tag{3}$$

The salt concentration balance equation

$$\phi_{sw}\dot{m}_{sw} = \phi_b \dot{m}_b + \phi_p \dot{m}_p^* \tag{4}$$

where ϕ_{sw}, ϕ_b, and ϕ_p are the seawater, brine, and products salinities, respectively, and $\dot{m}_p^*$ is taken as $H_2O(g)$ (sum of the water vapor of products of combustion, $\dot{m}_{H2O(g),cp}$ and seawater evaporation, $\dot{m}_{wv}$). We solved Eqs. (1)-(4) for $\dot{m}_{sw}$, $\dot{m}_{wv}$, $\dot{m}_p$, and $\dot{m}_b$, then calculated $\dot{m}_{t,wv} = \dot{m}_{wv} + \dot{m}_{H2O(g),cp}$. In the calculations, $\phi_{sw} = 3.53\%$, $\phi_b = 10\%$, $\phi_p = 0.025\%$, $h_{sw} = 405.8kJ/kg$, $h_b = 381kJ/kg$, h_{cp} (at $T_{cp} = 1197K$, $T_{cp} = 1263K$, $T_{cp} = 423K$) were used and $\dot{m}_{cp}$ values were estimated experimentally from the combustion of C_3H_8 with air. As the fuel mass flow rates were relatively small in our preliminary experiments, $\dot{m}_{C3H8}$ values were taken 10 times as greater of those, or as $0.3\cdot10^{-3}$, $1.2\cdot10^{-3}$, $2.1\cdot10^{-3}$, $3.0\cdot10^{-3}\,kg/s$

Figures 2 and 3 show $\dot{m}_{wv}$ and $\dot{m}_{t,wv}$ changes with $\dot{m}_{cp}$ of C_3H_8 and H_2 fuels. $\dot{m}_{cp}$'s were calculated, respectively, for the C_3H_8-air combustion and H_2-air combustion with no dissociation or association in the products from

$$\dot{m}_{cp} = \dot{m}_{CO2} + \dot{m}_{H2O(g)} + \dot{m}_{N2} \tag{5}$$

$$\dot{m}_{cp} = \dot{m}_{H2O(g)} + \dot{m}_{N2} \tag{6}$$

where the right hand side represents the products gases out of combustions

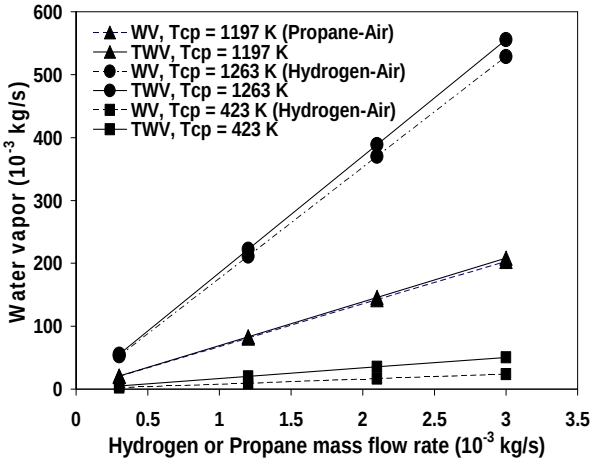

Figure 2. Water vapor mass flow rate with fuels mass flow rate (equal mass flow rate).

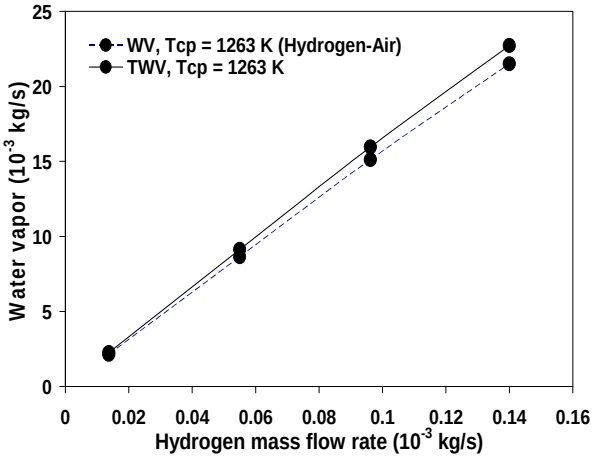

Figure 3. Water vapor mass flow rate with Hydrogen mass flow rate (equal mole flow rate).

LOCAL MODEL

In order to assess sizing parameters on the evaporator, a local evaporation model was used, which assumed 100% droplet evaporation (thus, $\dot{m}_b = 0g/s$, and $\dot{m}_{sw} = \dot{m}_{wv}$). Fig. 4 shows the ellipsoidal droplet used

in the current model. $r_o = 250\mu m$ and t_e was given for $r_o = 250\mu m$.

In the column, the dispersed phase denotes the seawater and the continuous phase denotes the combustion products. The model we used herein was similar to the one earlier given by (Elshaik, 1990) except in that the droplet shape we considered was ellipsoidal.

Considering the simplifying assumptions in Cartesian (x, y, z-) coordinates

$$v \cong 0,\ w \cong 0,\ \frac{\partial u}{\partial x} \cong 0 \tag{7}$$

Navier-Stokes equations in x-direction (on layer L) can be given as

$$0 = -\frac{dp}{dx} + \mu_v \frac{d^2 u}{dy^2} \tag{8}$$

where μ_v is the dispersed phase (seawater) vapor dynamic viscosity ($Pa \cdot s$). We assumed laminar flow regime inside the layer and μ_v was taken as constant. Integrating this equation under boundary conditions $u(0) = 0$ and $u(L) = 0$, we get

$$u = \frac{y}{2\mu_v}\frac{dp}{dx}(y - L) \tag{9}$$

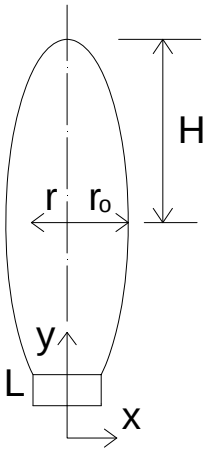

Figure 4. Ellipsoidal droplet and vapor layer on the ring element beneath, $r = r(t)$, $L = L(t)$, and $H = 3r_o$. The third dimension is also $r = r(t)$ and r_o

The mean velocity for the water vapor is

$$\bar{u} = \frac{1}{L}\int_0^L u dy \tag{10}$$

with Eq. (9)

$$\bar{u} = -\frac{L^2}{12\mu_v}\frac{dp}{dx} \tag{11}$$

Evaporation mass flow rate on the ring element in Fig. 4 can be written as

$$\bar{u}(2\pi x L)\rho_v = \dot{M}(\pi x^2) \tag{12}$$

where $\dot{M}$ is the mass flux ($kg/(s \cdot m^2)$), ρ_v is the dispersed phase density (kg/m^3). After combining the last two equations

$$\frac{dp}{dx} = -\frac{6\mu_v \dot{M} x}{\rho_v L^3} \tag{13}$$

and taking the integration for $x = r$, $p = 0$ (no vapor flow, $\bar{u} = 0$), we get

$$p(x) = \frac{3\mu_v \dot{M}}{\rho_v L^3}(r^2 - x^2) \tag{14}$$

where $r = r(t)$ and $0 \le x \le r$ in the course of evaporation. Writing a force balance on the droplet taking into account its weight

$$(\rho_l - \rho_v)Vg = \int_0^r p(2\pi x)dx \tag{15}$$

Substituting $p(x)$, we find

$$(\rho_l - \rho_v)g = \frac{3}{8}\frac{\mu_v \dot{M}}{\rho_v L^3} r \tag{16}$$

where ρ_l is the dispersed phase liquid density (kg/m^3), g is the gravitational acceleration ($g = 9.81 N/kg$), r ($= r(t)$) is the mean droplet width (m), and $V = \frac{4\pi}{3}3r^3$ is the droplet volume (m^3). Rate of evaporation was given on single droplet as

$$\rho_l \frac{dV}{dt} = -\pi r^2 \dot{M} \tag{17}$$

Plugging $V = \frac{4\pi}{3}3r^3$ and integrating between r_o and r

$$r = r_o - \frac{\dot{M}}{12\rho_l}t \tag{18}$$

which gives the decay of r_o during evaporation. In addition, heat given to the droplets by the combustion products

$$\dot{Q} = h_c A_s (T_{cp} - T_s) \tag{19}$$

and the required heat for the droplets evaporation is

$$\dot{Q} = \dot{M} A_b h_{fg} \tag{20}$$

in which h_c is the convective heat transfer coefficient for the combustion products ($W/(m^2K)$), A_s is the surface area of the ellipsoidal droplet from the Knud Thomsen formula ($p = 1.6075$, with a relative error $\leq$ 1.061%) (m^2), T_{cp} is the combustion products temperature (K), T_s is the saturation temperature for the dispersed phase at $p = 101.325kPa$ ($T_s = 373.15K + BPR(0.28K)$) where BPR is the seawater boiling point rise (Billet, 1989; Wark, 1995), A_b is the area beneath the seawater droplet (m^2), and h_{fg} is the latent heat of vaporization for the dispersed phase (kJ/kg). Equating last two equations

$$\dot{M} = \frac{4h_c\left(\frac{2\cdot 3^{1.6075}+1}{3}\right)^{0.622}(T_{cp} - T_s)}{h_{fg}} \tag{21}$$

and substituting into Eq. (18), we find

$$r = r_o - \frac{h_c\left(\frac{2\cdot 3^{1.6075}+1}{3}\right)^{0.622}(T_{cp} - T_s)}{3\rho_l h_{fg}} t \tag{22}$$

In order to determine the decay of droplet volume, we substitute Eqs. (21) and (22) into Eq. (17) and integrate between $V(0) = V_o$ and $V(t) = V$ to get

$$V - V_o = -\frac{4\pi h_c\left(\frac{2\cdot 3^{1.6075}+1}{3}\right)^{0.622}(T_{cp} - T_s)}{\rho_l h_{fg}} \times \int_0^t \left(r_o - \frac{h_c}{3\rho_l h_{fg}}\left(\frac{2\cdot 3^{1.6075}+1}{3}\right)^{0.622}(T_{cp} - T_s)t \right)^2 dt \tag{23}$$

Evaporation times calculated via Eqs. (22) and (23) were identical. The seawater mass flow rate was calculated due to the sensible cooling of the combustion products

$$\frac{\dot{m}_{sw}}{\dot{m}_{cp}} = \frac{c_{p,cp}(T_{cp} - T_s)}{h_{fg}} \tag{24}$$

where $c_{p,cp}$ is the specific heat for the combustion products ($kJ/(kgK)$): $c_{p,cp}$ was evaluated at $\Delta T_m = \frac{1}{2}(T_{cp} + T_s)$ and $\dot{m}_{cp}$s were calculated as in Eqs. (5) and (6) with no dissociation or association in reactions

The cross-section area of the evaporator was given based on the properties of the combustion products

$$A_e = \frac{\dot{m}_{cp}}{\rho_{cp}(1 - \varepsilon_d)v_{cp}} \tag{25}$$

where ρ_{cp} is the density of the combustion products (kg/m^3), v_{cp} is the velocity of the combustion products (m/s), and ε_d is the void fraction defined as the ratio of the volume of dispersed phase to that of total evaporator volume (-). Taking into account the fact that the evaporator is occupied by the dispersed and continuous phases throughout

$$\varepsilon_d = \frac{1}{1 + \frac{\rho_{sw}}{\rho_{cp}}\frac{\dot{m}_{cp}}{\dot{m}_{sw}}} \tag{26}$$

with

$$\rho_{sw} = \frac{\rho_f + \rho_v}{2}, \quad \rho_{cp} = \frac{p_{atm}}{R_{cp}\left(\frac{T_{cp} + T_s}{2}\right)} \tag{27}$$

In order to find the evaporation length, Δx_e

$$\Delta x_e = U_R t_e \tag{28}$$

where

$$U_R = \frac{v_d}{\varepsilon_d} - \frac{v_c}{1 - \varepsilon_d} \tag{29}$$

and $v_d = \dot{m}_{sw}/(\rho_{sw} A_e)$ and $v_c = \dot{m}_{cp}/(\rho_{cp} A_e)$ inside the evaporator column. Hence, through Eqs. (25) and (28), the evaporator volume was estimated

$$V_e \cong A_e \Delta x_e \tag{30}$$

Lastly, the volumetric heat transfer coefficient (U_v) was calculated from

$$U_v = \frac{Ua}{V_e} = \frac{\dot{m}_{sw} h_{fg}}{V_e \cdot LMTD} \tag{31}$$

or,

$$\dot{m}_{sw} h_{fg} = U_v V_e \cdot LMTD \tag{32}$$

a being the effective heat transfer surface area (m^2) and $U \cong h_c$. The fact ($U \cong h_c$) is due to the two factors: First is the absence of the heat transfer resistance of the heat transmitting material and second is the negligible heat transfer resistance of the dispersed phase compared to the combustion products (Kreith and Boehm, 1988). Logarithmic mean temperature difference ($LMTD$) was defined as

$$LMTD = \frac{(T_{cp} - T_{sw}) - (T_p - T_{sw})}{\ln \dfrac{T_{cp} - T_{sw}}{T_p - T_{sw}}} \tag{33}$$

In using $LMTD$, the products were assumed to exit the evaporator as superheated at $T_p = 375K$

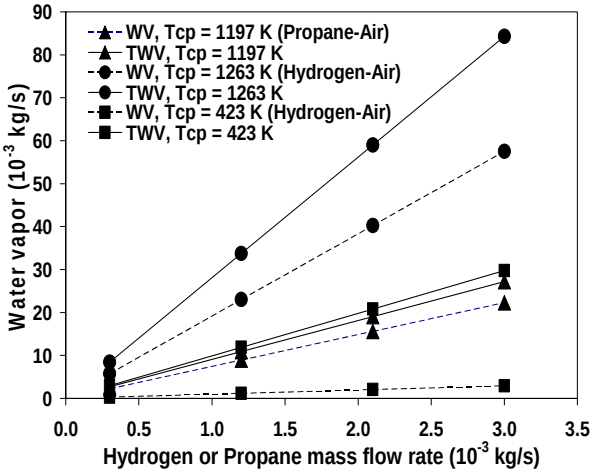

Figure 5. Water vapor mass flow rate with fuels mass flow rate (equal mass flow rate).

We present local model results $\dot{m}_{wv}$, $\dot{m}_{t,wv}$, A_e, t_e, Δx_e, and V_e in Figs. (5)- (16). In Figs. (5) and (6), $\dot{m}_{wv}$ and $\dot{m}_{t,wv}$ increase with $\dot{m}_{H2}$ or $\dot{m}_{C3H8}$ due to the total enthalpy carried away by the combustion products, or $\dot{m}_{cp}$. The effect of void fraction (ε_d) on the cross- section area of the evaporator is shown in Fig. (7). ε_d values were less than 0.1% for the Propane-air combustion ($T_{cp} = 1197K$), Hydrogen-air combustion ($T_{cp} = 1263K$), and Hydrogen-air combustion ($T_{cp} = 1263K$, equal mole flow rate) and less than 0.01% for the Hydrogen-air combustion ($T_{cp} = 423K$). These results indicate that indeed the dispersed phase occupies only a small fraction of the total evaporator volume.

In Figs. (8)-(11), Δx_e was seen to decrease with h_c; t_e values was nearly the same for $T_{cp} = 1197K$ and $T_{cp} = 1263K$ which substantially differed for $T_{cp} = 423K$ (See Fig. 12). As h_c increased, V_e was seen to decrease. This was shown in Figs. (13)-(16). Results in Figs. (8)- (16) were included for uniform (constant) h_c values. In the course of evaporation, h_c changes were reported for a bubble column design (Kendoush, 2004) and the references therein.

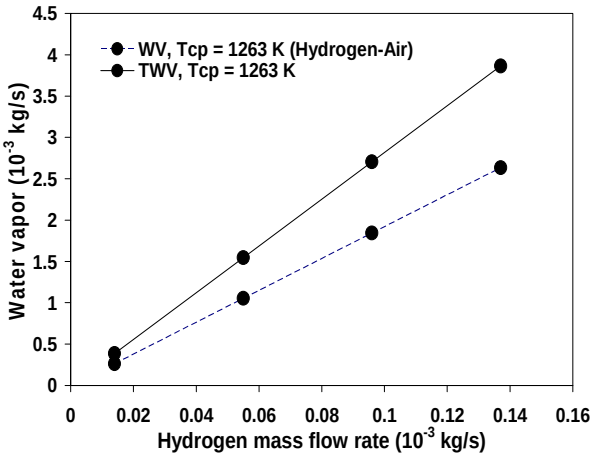

Figure 6. Water vapor mass flow rate with fuel mass flow rate (equal mole flow rate).

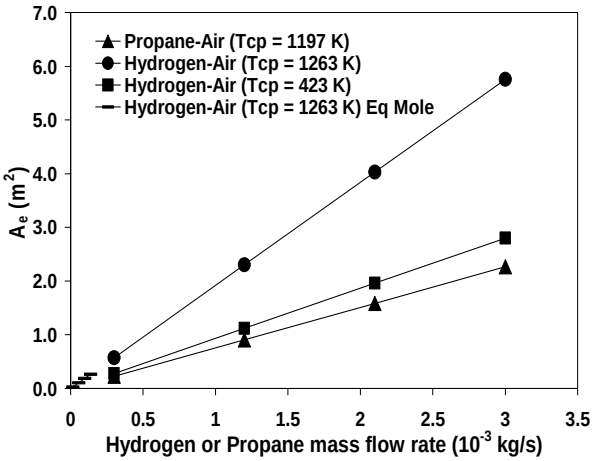

Figure 7. Evaporator cross-section area versus fuels mass flow rate.

Larger values for $\dot{m}_{wv}$ in Figs. (2) and (3) versus Figs. (5) and (6) was due to the properties of the combustion products evaluated at T_{cp} (global model) versus T_m (local model). Heat of vaporization (h_{fg}) values directly plugged into the local model resulted in small values for $\dot{m}_{wv}$

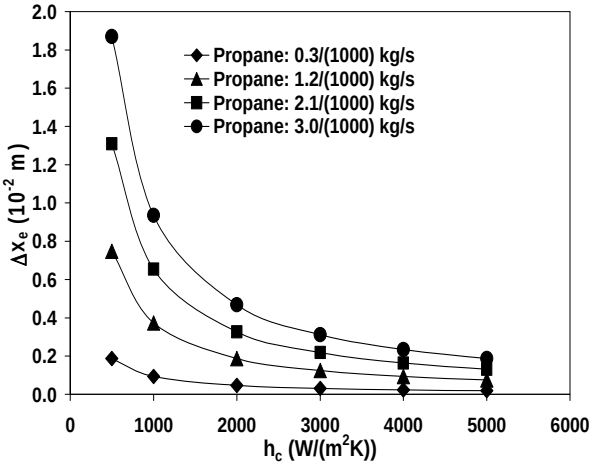

Figure 8. Evaporation length versus heat transfer coefficient, Propane-air combustion ($T_{cp} = 1197K$).

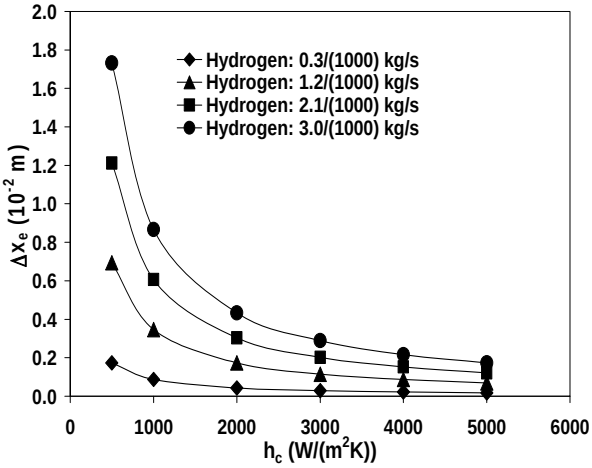

Figure 9. Evaporation length versus heat transfer coefficient, Hydrogen-air combustion ($T_{cp} = 1263K$).

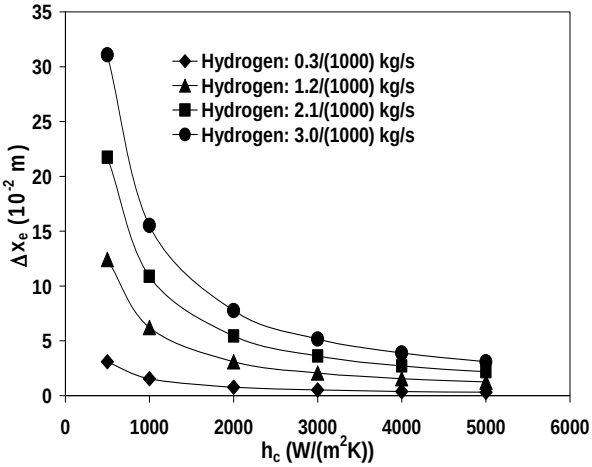

Figure 10. Evaporation length versus heat transfer coefficient, Hydrogen-air combustion ($T_{cp} = 423K$).

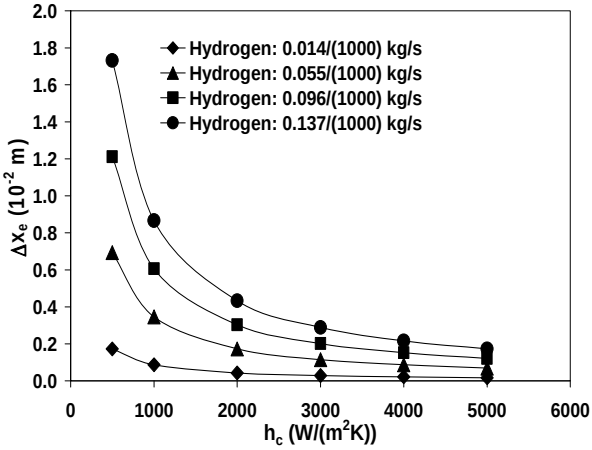

Figure 11. Evaporation length versus heat transfer coefficient, Hydrogen-air combustion, equal mole flow rate with $T_{cp} = 1263K$.

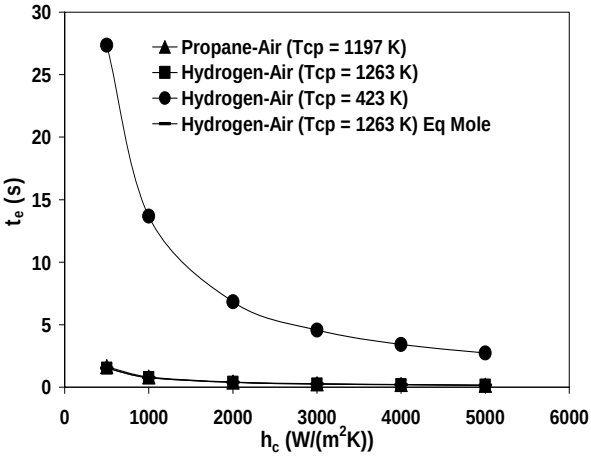

Figure 12. Evaporation time versus heat transfer coefficient for the fuels.

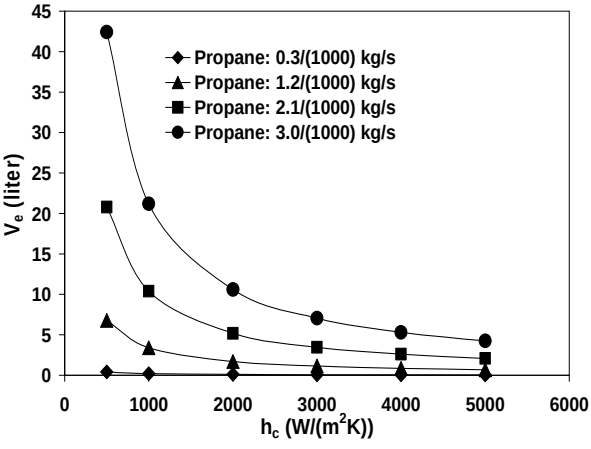

Figure 13. Evaporator volume versus heat transfer coefficient for Propane-air combustion ($T_{cp} = 1197K$).

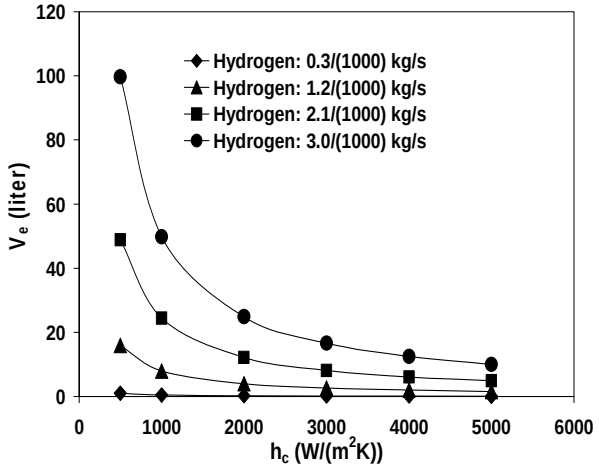

Figure 14. Evaporator volume versus heat transfer coefficient for Hydrogen-air combustion ($T_{cp} = 1263K$).

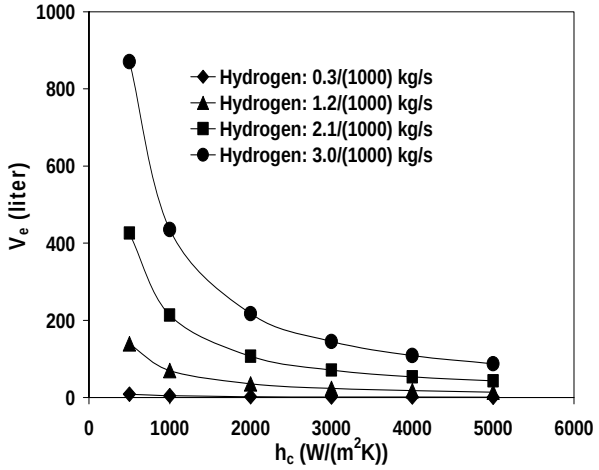

Figure 15. Evaporator volume versus heat transfer coefficient for Hydrogen-air combustion ($T_{cp} = 423K$).

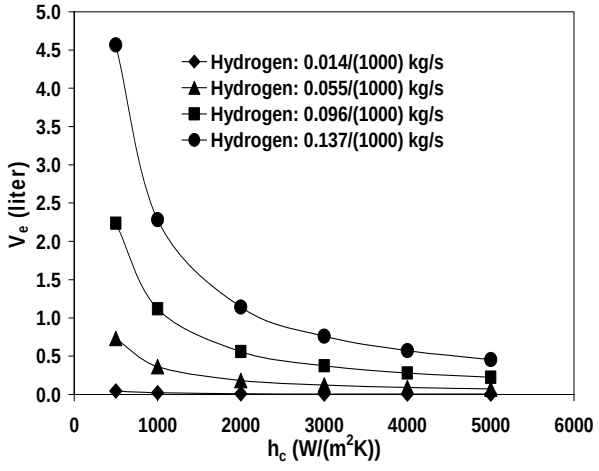

Figure 16. Evaporator volume versus heat transfer coefficient for Hydrogen-air combustion, equal mole flow rate with $T_{cp} = 1263K$.

CONCLUSIONS

We developed two heat transfer models and evaluated the effectiveness of a direct-contact heat exchange process in desalination of seawater. A spray- column was focused on. The spray-column evaporation shows unique fluid dynamics characteristics compared to a bubble column design and the process inside the present spray-column somewhat resembles a swamp cooler. From our global model centering on first law of thermodynamics, we showed that about 65% of the incoming seawater evaporation was possible. This defined the recovery ratio ($\dot{m}_{wv} / \dot{m}_{sw}$) of the seawater evaporation process.

Local model centering on Navier- Stokes Eqs. was used to estimate the sizing on the heat exchanger including evaporator length, cross-section area, and volume. It was found that for a given enthalpy of the combustion products, only certain amount of seawater can evaporate, thereby, be desalinated. Increasing T_{cp} was found to turn out lower Δx_e , t_e , and V_e but increase $\dot{m}_{sw}$, $\dot{m}_{wv}$, and U_v .

The other similar methods of thermal distillation, with lower yields compared to MSF and RO processes, include distillation via freezing and solar humidification

An efficient direct- contact heat transfer process was proposed in desalination of seawater. Experimental testing is crucial to validate the process, which may initially substitute a cheaper fuel, e.g., a hydrocarbon.

ACKNOWLEDGEMENTS

The author thanks to Dr. Byard D. Wood through the U.S. Bureau of Reclamation and U.S. Department of Energy for their support on this project.

REFERENCES

Billet, R., *Evaporation Technology*, VCH Publishers, New York, 1989.

Elshaik N. M., *Direct Contact Heat Transfer to a Dispersed Droplet with Change of Phase*, North Carolina State University, Dissertation thesis, 1990.

Hsu, S. T., Cheng, K. T., and Chiou, J. S., Seawater Desalination by Direct Contact Membrane Distillation, *Desalination* 143, 279-287, 2002.

International Desalination Association (IDA), 2000. Available at http://www.idadesal.org/

Kendoush, A. A., Theory of Convective Drop Evaporation in Direct Contact with an Immiscible Liquid, *Desalination* 169, 33–41, 2004.

Khawaji, A. D., Kutubkhanah, I. K., and Wie, J-M., Advances in Seawater Desalination Technologies, *Desalination* 221, 47–69, 2008.

Kreith, F. and Boehm, R. F., *Direct Contact Heat Transfer*, Hemisphere Pub Corp, Washington, 1988.

Marek, R. and Straub, J., Analysis of the Evaporation Coefficient and the Condensation Coefficient of Water, *Int. J. of Heat and Mass Transfer* 44, 39-53, 2001.

Termpiyakul, P., Jiraratananon, R., and Srisurichan, S., Heat and Mass Transfer Characteristics of a Direct Contact Membrane Distillation Process for Desalination, *Desalination* 177, 133-141, 2005.

Yun, Y., Ma, R., Zhang, W., Fane, A. G., and Li, J., Direct Contact Membrane Distillation Mechanism for High Concentration NaCl Solutions, *Desalination* 188, 251-262, 2006.

Wark, K., *Advanced Thermodynamics for Engineers*, McGraw-Hill, New York, 1995.

Murat TEKELİOĞLU received his B.Sc. degree in Mechanical Engineering from the Istanbul Technical University in 1998. He holds M.Sc. and Ph.D. degrees in Mechanical Engineering from the University of Nevada, Reno, earned in 2000 and 2005, respectively. His research interests include thermal, electrical, and optical systems design and simulation. He is an Assistant Professor of Mechanical Engineering Department in Karabük University and currently teaching at Gazi University in Ankara.